Research Article

ADVANCED PHOTONICS

Rydberg state excitation in molecules manipulated by bicircular two-color laser pulses

Wenbin Zhang,[a,b,c,*] Yongzhe Ma,[a] Chenxu Lu,[a] Fei Chen,[a] Shengzhe Pan,[a] Peifen Lu,[a] Hongcheng Ni,[a,d,*] and Jian Wu[a,d,e,*]

[a]East China Normal University, State Key Laboratory of Precision Spectroscopy, Shanghai, China
[b]Ludwig-Maximilians-Universität Munich, Department of Physics, Garching, Germany
[c]Max Planck Institute of Quantum Optics, Garching, Germany
[d]Shanxi University, Collaborative Innovation Center of Extreme Optics, Taiyuan, China
[e]CAS Center for Excellence in Ultra-Intense Laser Science, Shanghai, China

Abstract. Multiphoton resonant excitation and frustrated tunneling ionization, manifesting the photonic and optical nature of the driving light via direct excitation and electron recapture, respectively, are complementary mechanisms to access Rydberg state excitation (RSE) of atoms and molecules in an intense laser field. However, clear identification and manipulation of their individual contributions in the light-induced RSE process remain experimentally challenging. Here, we bridge this gap by exploring the dissociative and nondissociative RSE of H_2 molecules using bicircular two-color laser pulses. Depending on the relative field strength and polarization helicity of the two colors, the RSE probability can be boosted by more than one order of magnitude by exploiting the laser waveform-dependent field effect. The role of the photon effect is readily strengthened with increasing relative strength of the second-harmonic field of the two colors regardless of the polarization helicity. As compared to the nondissociative RSE forming H_2^*, the field effect in producing the dissociative RSE channel of (H^+, H^*) is moderately suppressed, which is primarily accessed via a three-step sequential process separated by molecular bond stretching. Our work paves the way toward a comprehensive understanding of the interplay of the underlying field and photon effects in the strong-field RSE process, as well as facilitating the generation of Rydberg states optimized with tailored characteristics.

Keywords: strong-field Rydberg state excitation; molecular dissociative ionization; bicircular two-color fields; multiphoton resonant excitation; frustrated tunneling ionization.

Received Oct. 4, 2022; revised manuscript received Dec. 8, 2022; accepted for publication Dec. 21, 2022; published online Jan. 10, 2023.

[DOI: 10.1117/1.AP.5.1.016002]

1 Introduction

Benefiting from their unique properties, such as extremely large electron orbital radius and low electron binding energy, Rydberg atoms or molecules have a huge potential for applications in a wide range of fields, from quantum physics and chemistry to astrophysics.[1–3] For instance, they can serve as building blocks for advanced technologies in precision measurements,[4] quantum information processing,[5] quantum nonlinear optics,[6] and long-range many-body interactions.[7,8] In particular, the Rydberg state excitation (RSE) of atoms or molecules driven by intense laser fields has a plethora of exciting applications, including accelerating and de-accelerating neutral particles,[9,10] generating near-threshold harmonics[11] and coherent extreme-ultraviolet light emission,[12] and realizing multiphoton Rabi oscillations.[13]

In analogy to the multiphoton and tunneling mechanisms proposed for photoionization, the strong-field RSE of atoms or molecules can be accessed via either resonant multiphoton excitation[14–18] or electron recapture excitation.[19–31] These two scenarios illustrate the individual photon and field contributions of the driving light to the RSE via direct photon absorption or electron recapture, termed as the "photon effect" and "field

*Address all correspondence to Wenbin Zhang, wenbin.zhang@physik.uni-muenchen.de; Hongcheng Ni, hcni@lps.ecnu.edu.cn; Jian Wu, jwu@phy.ecnu.edu.cn

effect," respectively. In the photon point of view, the atoms or molecules are resonantly excited to the Rydberg states by simultaneously absorbing multiple photons, which is primarily governed by the photon energy of the incident light. Alternatively, in the field scenario, the electron tunnels through the laser-dressed Coulomb barrier, quivers in the oscillating laser field, and may be recaptured into the Rydberg orbitals of the parent ion after the conclusion of the laser pulse.[20,21] Depending on the laser parameters, e.g., the field intensity, wavelength, and polarization, both the photon and field effects have been observed in the strong-field RSE of atoms[14–17,21,29] and molecules.[18,19,22–28,30] For instance, the RSE accessed via the photon scenario has been observed at short wavelengths and low intensities regardless of the laser polarization.[18,19] In contrast, since the trajectory of the tunneled electron critically depends on the detailed waveform of the laser field, the electron-recapture-induced RSE occurs in a linearly polarized laser field but is suppressed in circular polarization, in which case electrons are driven away from the ionic cores.[21] In principle, the photon and field effects coexist and both contribute to the RSE, even when one of them is dominant.[31,32] While they serve as the cornerstone to understand and control the strong-field RSE of atoms and molecules, an unambiguous identification of the individual contributions of the photon and field effects, however, is experimentally challenging, and has not been achieved so far. Here, we bridge this gap and report an experimental demonstration of disentangling and controlling the photon and field effects in RSE of a H_2 molecule by employing bicircular two-color (BCTC) laser fields.

The BCTC laser fields have attracted considerable attention in steering two-dimensional directional bond breaking,[33] manipulating the electron-ion rescattering[34] and nonsequential double ionization (NSDI),[35–38] generating circularly polarized extreme ultraviolet light,[39–41] and spatially controlling surface reactions on nanoparticles at the nanoscale.[42] Past studies using BCTC laser fields mostly focused on the atomic and molecular ionization dynamics.[33–42] Until recently, the excitation dynamics of atoms and molecules via frustrated tunneling ionization[21] were theoretically studied with BCTC laser pulses, which, however, only takes into account the field effect.[43,44] In this article, we use these versatile BCTC laser fields to experimentally investigate the strong-field RSE of H_2 molecules, where the created Rydberg fragments are measured and identified in the coincidence measurements. Studying the yield probabilities of the nondissociative ($H_2 + n\hbar\omega \rightarrow {H_2}^*$, denoted as ${H_2}^*$) and dissociative [$H_2 + n\ \ \omega \rightarrow H^+ + H^* + e^-$, denoted as (H^+, H^*)] RSE channels versus the relative field strength and polarization helicity of the two colors, we clearly determine the individual contributions of the field and photon effects. For a given relative field strength of the two colors, the electron recapture process facilitated by the field effect of the driving light is switched on or off by switching the polarization of the BCTC fields from counterrotating to co-rotating, whereas the contribution of the photon effect in the RSE yield remains comparable. The observed yield difference in the counterrotating field as compared to the co-rotating case therefore qualitatively gives the contribution of the field effect in producing the corresponding RSE channels. By finely adjusting the relative field strength of the two colors, we can manipulate the waveform of the laser field and the number of photons participating in the RSE processes and thus the relative contributions of the field and photon effects.

2 Experimental Methods

In our experiment, as schematically illustrated in Fig. 1(a), the BCTC laser fields were generated by spatiotemporally overlapping two circularly polarized fundamental wave (FW) and second-harmonic (SH) pulses using a Mach–Zehnder interferometer. The SH pulse was created by frequency doubling the linearly polarized FW laser pulse (25 fs, 790 nm, and 10 kHz) in a β-barium borate crystal. Followed by the independent circular polarization shaping in two arms of the interferometer, the FW and SH pulses with the opposite or same polarization helicity were recombined using a dichromatic mirror to produce counterrotating or co-rotating two-color laser fields. The BCTC laser pulses were focused onto the supersonic gas jet of H_2 in the apparatus of cold target recoil ion momentum spectroscopy (COLTRIMS).[45,46] The peak intensities in the focus for the two colors, i.e., I_{FW} and I_{SH}, were calibrated separately by examining the proton momentum spectrum for the FW pulses[47] and tracing the field-intensity-dependent energy shift of the discrete above threshold ionization spectrum of H_2 for SH pulses.[48] The intensities can be adjusted individually via the neutral filters installed in each beam arm before their collinear recombination.

By measuring the electron, ion, and excited neutral Rydberg atom in coincidence, the COLTRIMS apparatus allows us to unambiguously identify the RSE channels of ${H_2}^*$ and (H^+, H^*). As shown in Fig. 1(b), the ${H_2}^*$ channel can be identified in the photoelectron–photoion coincidence (PEPICO) spectrum,[19,29,49] which is measured on the basis of the postpulse field ionization of the laser-induced Rydberg states,[50–52] whereas the (H^+, H^*) pair can be discriminated in the photoion–photoion coincidence (PIPICO) spectrum,[53] as shown in Fig. 1(c). We note that the strong-field-induced neutral dissociation of H_2 through superexcited states,[54] accompanied by further ionization of neutral fragments, has a negligible effect on our measurements. More details of the experimental methods and the information on the principle quantum number of the measured Rydberg fragments are presented in the Supplementary Material.

3 Results and Discussion

Figure 2(a) shows the measured yields of the ${H_2}^*$ and (H^+, H^*) channels in the counterrotating and co-rotating BCTC fields as a function of the relative-field strength E_{SH}/E_{FW} of the two colors. In the measurements, the intensity of the combined laser fields, i.e., $I_c = (\sqrt{I_{SH}} + \sqrt{I_{FW}})^2$, was kept constant $\sim 6.0 \times 10^{14}\ \mathrm{W/cm^2}$ for various field ratios. This allows one to minimize the intensity-dependent photon spin effects originating from different field helicities on the ionization and excitation processes[55] and also to obtain a proper event rate for data acquisition. This is confirmed by the nearly flat and helicity-independent single-ionization yields of ${H_2}^+$ (see Supplementary Material). Each data point is normalized per laser shot over more than 10^8 shots. The relative collection and detection efficiencies for different fragmental species have been taken into account.[53,56] As shown in Fig. 2(a), noticeable yields of the ${H_2}^*$ (red open circles) and (H^+, H^*) (blue open squares) channels are clearly observed in the co-rotating bicircular fields, which are mostly accessed via the multiphoton excitation process, since the electron recapture process is suppressed here. The yields of ${H_2}^*$ and (H^+, H^*) both increase rapidly when the field ratio E_{SH}/E_{FW} is increased from 0.5 to 2.0, followed by a broad plateau. This indicates that the contribution of photon effect in the RSE is boosted with the increase of the relative strength of the

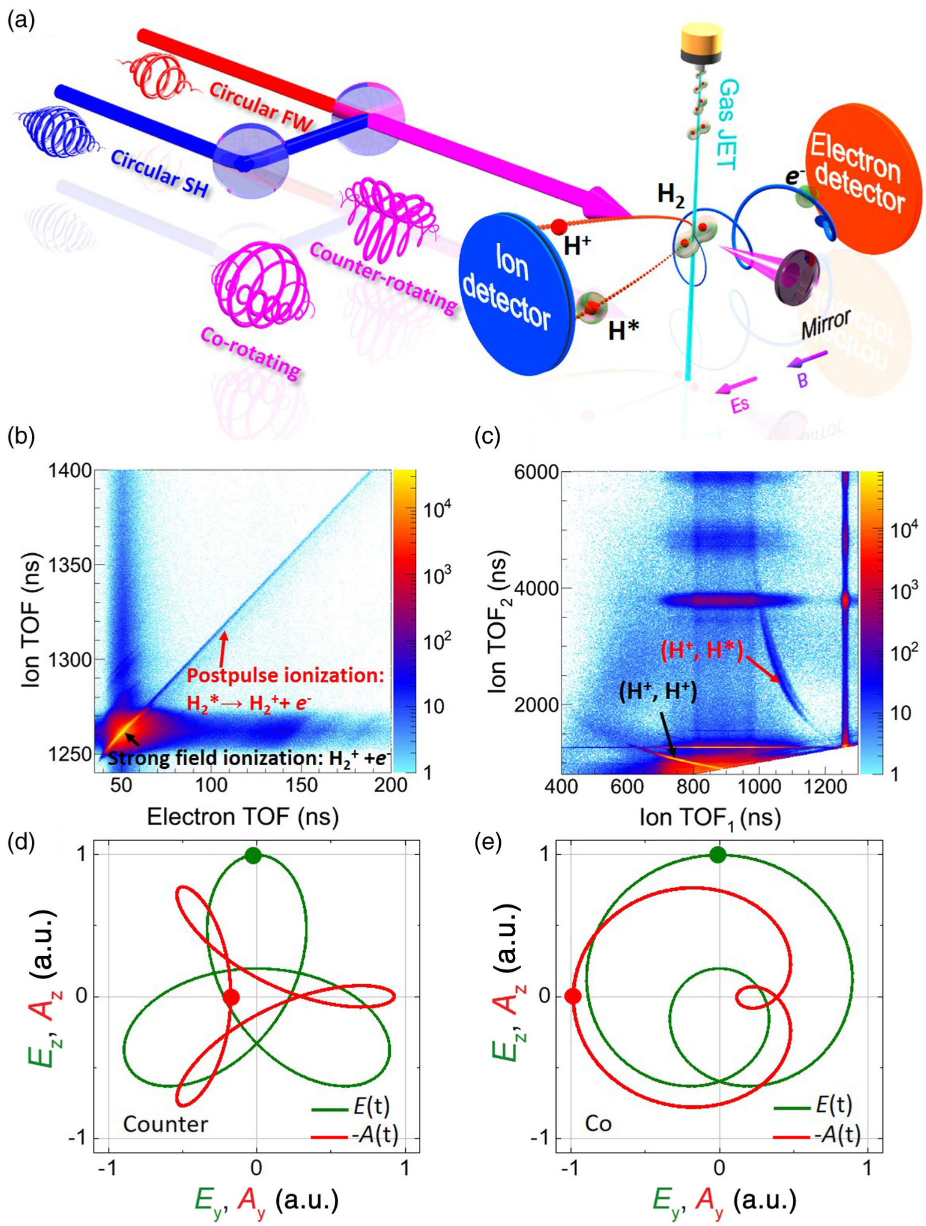

Fig. 1 Experimental scheme. (a) Schematic illustration of the experimental setup to study the RSE of the H_2 molecules with BCTC laser fields. (b), (c) Measured (b) PEPICO and (c) PIPICO spectrum of the H_2 molecule. The H_2^+ signals created from the postpulse ionization of $H_2{}^*$ and from the strong-field ionization H_2 can be distinguished in the PEPICO spectrum, while the (H^+, H^*) and (H^+, H^+) channels can be unambiguously identified in the PIPICO spectrum. (d), (e) Combined electric fields E_y versus E_z as well as the corresponding vector potential A_y versus A_z for the (d) counterrotating and (e) co-rotating circularly polarized two-color laser fields with a field ratio of $E_{SH}/E_{FW} = 1.5$.

SH field. The reason for this enhancement is that the photon energy of the SH field is 2 times that of the FW field. Therefore, for a given RSE channel, fewer photons are required with an increasing ratio E_{SH}/E_{FW}, leading to increased accessibility of the multiphoton excitation process. When multiphoton excitation already dominates RSE, a further increase in the relative strength of the SH field only leads to a minor rise in the excitation probability, leading to the observed nearly flat $H_2{}^*$ and (H^+, H^*) yields at $E_{SH}/E_{FW} > 2.0$. It is because the "share" of the SH portion in the total laser field does not increase much beyond this field ratio.

By switching the polarization helicity of the BCTC field from co-rotating to counterrotating, as shown in Fig. 2(a), the yields of the $H_2{}^*$ (red solid circles) and (H^+, H^*) (blue solid squares) channels are significantly enhanced (by more than one order of magnitude for $H_2{}^*$). In the counterrotating field, both the photon and field effects contribute, and thus the RSE yields are overall higher than that of the co-rotating case, where the

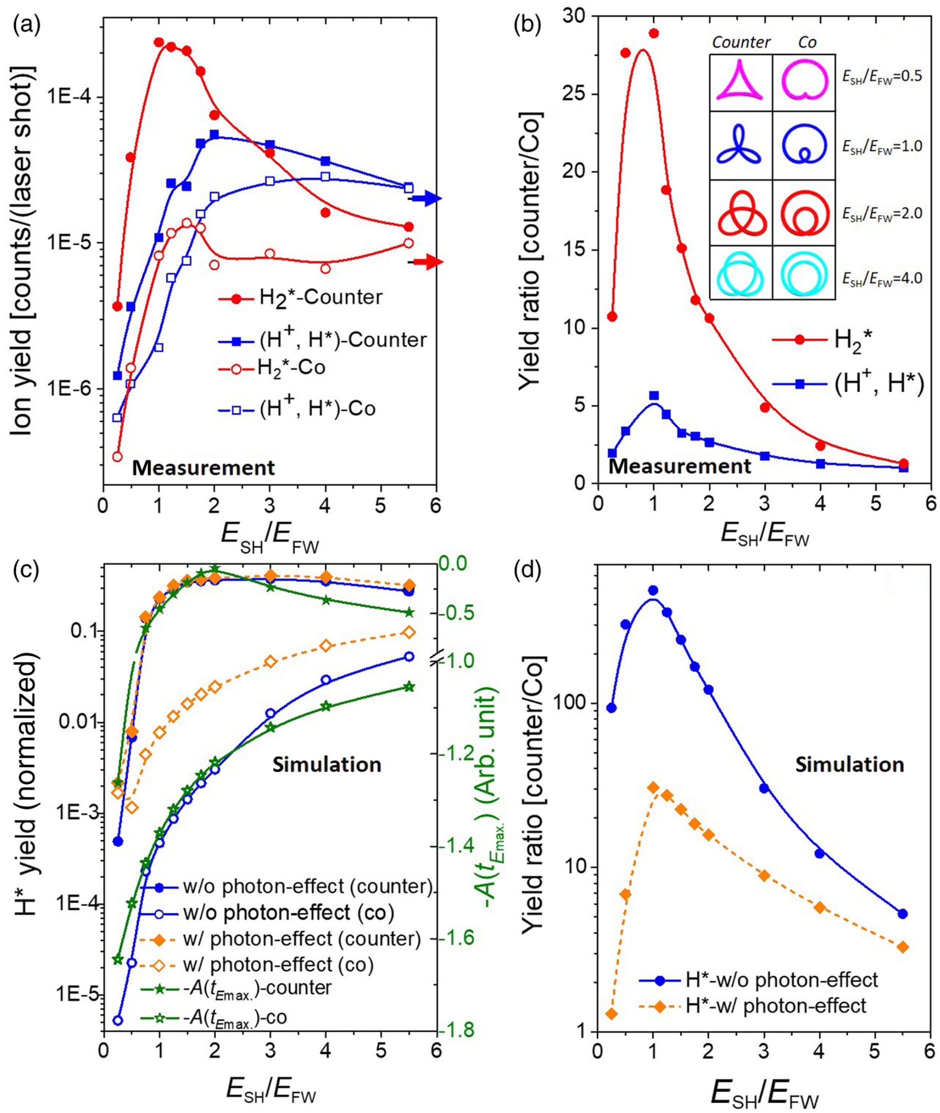

Fig. 2 Manipulation of RSE yield by BCTC laser pulses. (a) Experimentally measured yields of the Rydberg fragments of H_2^* and (H^+, H^*) channels created in the interaction of the H_2 molecules with BCTC laser fields. Solid and open symbols represent the counterrotating and co-rotating cases, respectively. The thick arrows near the right ordinate indicate the measured yield of the H_2^* and (H^+, H^*) channels employing a single-color SH circularly polarized laser pulse. The yield of each data point is normalized to a single laser shot. (b) The corresponding yield ratios between the counterrotating and co-rotating cases of the RSE channels displayed in panel (a). The shapes of combined electric fields of the BCTC fields for different field ratios and polarization helicities are illustrated in the inset of panel (b). (c) Numerically simulated Rydberg yields of H^* for the counterrotating and co-rotating cases of the BCTC laser pulse. The yield of each data point is normalized to the simulated total number of released electrons. The right ordinate shows the inverse of the magnitude of the vector potential $[-A(t)]$ of the counterrotating and co-rotating fields where the field amplitude maximizes. The case without the photon effect is shown in blue, and the other case with the photon effect included is shown in orange. (d) The corresponding yield ratios between the counterrotating and co-rotating cases of the simulated Rydberg yield of H^* for the two cases in panel (c).

field effect is significantly suppressed. For a given E_{SH}/E_{FW} ratio, the contribution of the photon effect is comparable in the counterrotating and co-rotating fields; the strikingly enhanced RSE probability in the counterrotating field is thus attributed to the contribution of the field effect. To increase the visibility of the enhancement and quantify the contribution of the field effect as compared to that of the photon effect, in Fig. 2(b), we plot the measured yield ratios of the RSE channels between the counterrotating and co-rotating cases. Noticeable enhancements of both the H_2^* and (H^+, H^*) channels are observed around $E_{\mathrm{SH}}/E_{\mathrm{FW}} = 1.0$, with increment factors of ~ 28 and ~ 5, respectively, suggesting a crucial role of the field effect in boosting the RSE in the counterrotating BCTC laser fields.

The enhancement observed here is similar to the previous observations of the field-ratio-dependent NSDI probability of atoms and molecules in the sense of the control offered by the BCTC laser fields, where the enhanced double ionization is dominated by the electron recollision.[38–40] Owing to the peculiar waveform of the counterrotating two-color fields, the tunneled electron will initially be driven away but later be driven back to the parent ion. The two-dimensional close loop trajectory results in a much higher probability for the electron to re-encounter the parent ion, giving rise to the NSDI. The situation is a bit different for the RSE here. In contrast to NSDI, the trajectory of the electron does not have to return to the parent ion, but needs to have a small velocity after the conclusion of the laser field, such that the electron can be captured into a Rydberg orbital. As illustrated in Fig. 1(d), in the counterrotating bicircular laser field, the magnitude of the vector potential features a local minimum (red dot) where the electric field is at a local maximum (green dot) of its magnitude, so that the electron with a maximal tunneling probability will end up with a small final velocity. Such a property of the counterrotating bicircular field leads to a prominent field effect in generating RSE. This observation is again in line with the properties of the counterrotating field, since the local minimum in the magnitude of the vector potential can be lowered by optimizing the field ratio, as plotted in Fig. 2(c) (green solid stars). In contrast, for the co-rotating field, as shown in Fig. 1(e), the vector potential has a local maximum (red dot) in its magnitude where the electric field peaks (green dot), which strongly suppresses electron recapture.

The much higher increment of the $H_2{}^*$ channel compared to that of the (H^+, H^*) channel, as shown in Fig. 2(b), implies that the field effect plays a more dominant role in producing the $H_2{}^*$ as compared to the (H^+, H^*) channel. To illuminate the difference between the relative roles of the field and photon effects in producing the $H_2{}^*$ and (H^+, H^*) channels, we turn to inspect the accessing dynamics of these two channels.

In the electron recapture scenario, driven by the field effect of the counterrotating bicircular field, $H_2{}^*$ can be formed if the tunneled electron with negligible kinetic energy is recaptured by the parent ion $H_2{}^+$, while for the generation of the (H^+, H^*) channel,[53,57,58] the ionization-created nuclear wave packet of $H_2{}^+$ needs to stretch to a critical internuclear distance ($R \sim 10$ a.u.), where the charge-resonance-enhanced ionization occurs to boost the tunneling of the second electron.[59] The tunneled electron is subsequently recaptured by one of the outgoing H^+ ions of the Coulomb explosion double ionization channel, i.e., $H_2 + n\quad\omega \to H^+ + H^+ + 2e^-$ [denoted as (H^+, H^+)]. By considering the kinetic energy release (KER) of the observed (H^+, H^*) channel, we estimate a bond stretching time of about 25 fs for the nuclear wave packet propagating from $R \sim 1.4$ a.u. (the equilibrium internuclear distance of H_2) to ~ 10 a.u. on the potential energy curves of H_2^+. Therefore, the tunneling of the second electron at the critical internuclear distance mostly occurs at the trailing edge of the bicircular laser pulse where the field strength is moderately weak. It results in a lower probability in producing the (H^+, H^*) channel as compared to that of the $H_2{}^*$ channel, in which the electron tunneling mostly occurs around the peak of the laser pulse. It explains the much larger increment of the yield of $H_2{}^*$ than that of the (H^+, H^*) channel, as shown in Fig. 2(b), where the enhancement is facilitated by the electron recapture process with a maximal efficiency around field ratio of $E_{\mathrm{SH}}/E_{\mathrm{FW}} \sim 1$ in the counterrotating BCTC laser pulse.

In contrast, in the multiphoton excitation scenario, the RSE is accessed by directly absorbing multiple photons from the laser field, which will be considerably boosted if multiphoton resonance occurs. As compared to the nondissociative $H_2{}^*$, the resonance excitation of the stretching $H_2{}^+$ to the (H^+, H^*) can always be fulfilled with the energy of a certain number of photons matching the potential energy gap between the $2p\sigma_u$ state and the repulsive Rydberg states at proper internuclear distances. As discussed above, the contribution of the photon effect increases with the rising field ratio $E_{\mathrm{SH}}/E_{\mathrm{FW}}$ for a constant combined laser intensity. This is more obvious in the co-rotating bicircular field, where the electron recapture process is suppressed. As a result, as shown in Fig. 2(a), the yields of the (H^+, H^*) channel exceed that of the $H_2{}^*$ channel when the field ratio $E_{\mathrm{SH}}/E_{\mathrm{FW}} > 2.5$ and 1.75 for the counterrotating and co-rotating fields, respectively. At the first glance, it seems counterintuitive, since many more photons are required to access the (H^+, H^*) than $H_2{}^*$, which further confirms the importance of the resonance in the multiphoton excitation process. The fact that the yield of (H^+, H^*) surpasses that of $H_2{}^*$ with increasing field ratio $E_{\mathrm{SH}}/E_{\mathrm{FW}}$ is consistent with our measurement using a single circularly polarized SH field, which corresponds to the limiting case of $E_{\mathrm{SH}}/E_{\mathrm{FW}} \to \infty$.

As indicated by the thick arrows near the right ordinate of Fig. 2(a), driven by a single circularly polarized SH pulse with an intensity of $\sim 6.0 \times 10^{14}$ W/cm^2, the yield of (H^+, H^*) (2.0×10^{-5} counts/laser shot, blue arrow) is one order of magnitude higher than that of the $H_2{}^*$ (7.4×10^{-6} counts/laser shot, red arrow). In this scenario, the photon effect dominates ionization,[18,19] and the (H^+, H^*) channel is accessed via the following process: $H_2{}^+$ created upon photoionization first stretches on the $1s\sigma_g$ potential energy curve and transits to the $2p\sigma_u$ state by absorbing one SH photon via a $1\omega_{\mathrm{SH}}$ pathway, followed by a resonant excitation to the repulsive Rydberg state at an internuclear distance around 10 a.u., which eventually fragmentizes into a (H^+, H^*) pair with a KER ~ 4.0 eV, as indicated by the blue arrow pointing to the black dashed curve in Fig. 3(b). Alternatively, the stretching $H_2{}^+$ can also dissociate into a hydrogen atom and a proton, i.e., $H_2{}^+ + n\hbar\omega \to H^+ + H + e^-$ [denoted as (H^+, H)], via a comparable $1\omega_{\mathrm{SH}}$ pathway. As shown in Figs. 3(a) and 3(b), for the case using the co-rotating bicircular fields, the yields of the $1\omega_{\mathrm{SH}}$ pathway of the (H^+, H) channel (KER ~ 1.2 eV) and of the (H^+, H^*) channel (KER $\sim$ 4.0 eV) increase with rising SH field strength. It is consistent with the observed steep enhancement in the (H^+, H^*) yield, as shown in Fig. 2(a), as well as the (H^+, H) and (H^+, H^+) channels, as shown in Fig. S2(a) in the Supplementary Material, when the field ratio $E_{\mathrm{SH}}/E_{\mathrm{FW}}$ increases from 0.5 to 2. Accordingly, as shown in Fig. 3(a), the (H^+, H) channel with KER smaller than 0.5 eV produced via the $1\omega_{\mathrm{SH}} - 1\omega_{\mathrm{FW}}$ and $1\omega_{\mathrm{FW}}$ pathways is suppressed as the FW field strength decreases [see Fig. S3(a) in the Supplementary Material for the counterrotating case].

To further illuminate the photon and field effects in the strong-field RSE process, we take the simplest hydrogen atom to model the RSE process in the BCTC laser pulses by performing a classical trajectory Monte Carlo (CTMC) simulation, which accounts only for the field effect. More details of the simulation are presented in the Supplementary Material. As shown

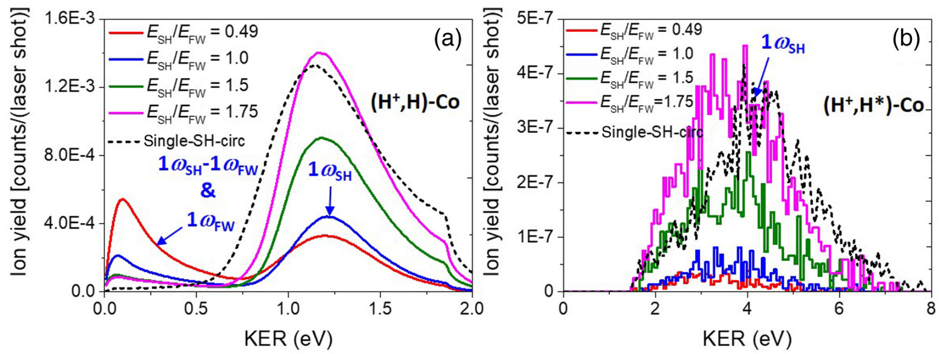

Fig. 3 Field-ratio-resolved KER spectra of the fragmentation channels in the co-rotating case. (a), (b) Measured KER distributions of the nuclear fragments of (a) the (H^+, H) channel and (b) the (H^+, H^*) channel using co-rotating BCTC laser fields at various E_{SH}/E_{FW} (colored solid curves) as well as applying single SH pulses (black dashed curves) with an intensity of $\sim 6.0 \times 10^{14}$ W/cm^2.

in Fig. 2(c), the experimentally observed field effect in accessing the strong-field RSE process is qualitatively reproduced (blue solid and open circles). It has a similar tendency to (the inverse of) the magnitude of the vector potential $[-A(t)$, green solid and open stars], where the electric field amplitude E maximizes [right ordinate of Fig. 2(c)], as expected for the field effect, which requires the final velocity to be small so that the tunneled electron can be recaptured. We note that due to the lack of photon effect in the CTMC simulation, a much higher yield ratio ($\sim$608) between the counterrotating and co-rotating cases is observed in Fig. 2(d) (blue solid circles). While a more sophisticated theoretical method (say, full three-dimensional time-dependent Schrödinger equation or the strong-field approximation generalized to apply to Rydberg excitation) is necessary to fully account for the photon effect, here we readily include the photon effect based on the simple physical intuition that the photon excitation probability should scale with the individual intensity of the two-color laser field to the power corresponding to the number of photons involved. With this in mind, we arrive at the yield of H^* with both field and photon effects, shown as orange solid and open squares in Figs. 2(c) and 2(d). For the counterrotating case, the field effect dominates, and adding the additional photon effect does not change the yield much. For the co-rotating case, the field effect is suppressed such that the contribution of the photon effect drastically enhances the yield, and reduces the ratio between the counterrotating and co-rotating cases to be around 32 [orange solid squares in Fig. 2(d)], arriving at a much better agreement with the experimental results of the ${H_2}^*$ channel. This additional contribution illustrates the importance of photon effects in a strong-field RSE process. In contrast, the large ratio between counterrotating and co-rotating cases, as shown in Fig. 2(d), confirms our conclusion that the field effect plays a crucial role in the underlying dynamics of the strong-field RSE process.

4 Conclusions

We have demonstrated that the bicircular laser fields of tunable relative strength and polarization helicity of the two colors not only support a precise control of the strong-field RSE dynamics, but also allow for an unambiguous discrimination of the individual contributions of the field and photon effects. Our findings show that both the field and photon effects play an important role in accessing the strong-field dissociative and nondissociative RSE of H_2 molecules, while the field effect is crucial in boosting the RSE in the counterrotating BCTC laser fields enabled by the tailored field shape. Our work with BCTC laser fields provides novel insights into the underlying mechanisms, i.e., the field effect versus the photon effect, of the RSE process and offers a promising route for manipulating the output of the RSE of atoms and molecules in intense laser fields.

Acknowledgments

This work was supported by the National Key R&D Program of China (Grant No. 2018YFA0306303), the National Natural Science Foundation of China (Grant Nos. 11834004, 61690224, 92150105, 11904103, 12241407, and 12227807), and the Science and Technology Commission of Shanghai Municipality (Grant No. 21ZR1420100). W. Zhang acknowledges the support from the Alexander von Humboldt Foundation. Numerical simulations were in part performed on the ECNU Multifunctional Platform for Innovation (001). We would like to acknowledge helpful discussions with Liang-Wen Pi. J. Wu coordinated and supervised this project. W. Zhang and J. Wu conceived and designed the experiments. W. Zhang, C. Lu, F. Chen, S. Pan, P. Lu, and J. Wu prepared and performed the measurements. W. Zhang and J. Wu analyzed and interpreted the experimental data. Y. Ma and H. Ni developed the theoretical model and carried out the calculation. All authors discussed the results and contributed to the final manuscript drafted by W. Zhang, H. Ni, and J. Wu. The authors declare no competing financial interests.

Data and Materials Availability

The data that support the plots within this article and other findings of this study are available from the corresponding author upon reasonable request.

References

1. M. Saffman, T. G. Walker, and K. Mølmer, "Quantum information with Rydberg atoms," *Rev. Mod. Phys.* **82**(3), 2313–2363 (2010).
2. J. P. Shaffer, S. T. Rittenhouse, and H. R. Sadeghpour, "Ultracold Rydberg molecules," *Nat. Commun.* **9**(1), 1965 (2018).
3. M. Y. Zakharov, N. N. Bezuglov, and A. N. Klycharev, "Rydberg atoms in astrophysics," *New Astron. Rev.* **53**, 259–265 (2009).

4. A. Facon et al., "A sensitive electrometer based on a Rydberg atom in a Schrodinger-cat state," *Nature* **535**(7611), 262–265 (2016).
5. L. Li, Y. O. Dudin, and A. Kuzmich, "Entanglement between light and an optical atomic excitation," *Nature* **498**(7455), 466–469 (2013).
6. T. Peyronel et al., "Quantum nonlinear optics with single photons enabled by strongly interacting atoms," *Nature* **488**(7409), 57–60 (2012).
7. V. Bendkowsky et al., "Observation of ultralong-range molecules," *Nature* **458**(7241), 1005–1008 (2009).
8. D. Maxwell et al., "Storage and control of optical photons using Rydberg polaritons," *Phys. Rev. Lett.* **110**(10), 103001 (2013).
9. U. Eichmann et al., "Acceleration of neutral atoms in strong short-pulse laser fields," *Nature* **461**(7268), 1261–1264 (2009).
10. S. D. Hogan, C. Seiler, and F. Merkt, "Rydberg-state-enabled deceleration and trapping of cold molecules," *Phys. Rev. Lett.* **103**(12), 123001 (2009).
11. W. Xiong et al., "Mechanisms of below-threshold harmonic generation in atoms," *Phys. Rev. Lett.* **112**(23), 233001 (2014).
12. H. Yun et al., "Coherent extreme-ultraviolet emission generated through frustrated tunnelling ionization," *Nat. Photonics* **12**(10), 620–624 (2018).
13. M. Fushitani et al., "Femtosecond two-photon Rabi oscillations in excited he driven by ultrashort intense laser fields," *Nat. Photonics* **10**(2), 102–105 (2016).
14. M. P. de Boer and H. G. Muller, "Observation of large populations in excited states after short-pulse multiphoton ionization," *Phys. Rev. Lett.* **68**(18), 2747–2750 (1992).
15. R. R. Jones, D. W. Schumacher, and P. H. Bucksbaum, "Population trapping in Kr and Xe in intense laser fields," *Phys. Rev. A* **47**(1), R49–R52 (1993).
16. G. N. Gibson, L. Fang, and B. Moser, "Direct femtosecond laser excitation of the 2p state of h by a resonant seven-photon transition in H_2^+," *Phys. Rev. A* **74**(4), 041401 (2006).
17. Q. Li et al., "Fine structures in the intensity dependence of excitation and ionization probabilities of hydrogen atoms in intense 800-nm laser pulses," *Phys. Rev. A* **89**(2), 023421 (2014).
18. W. Zhang et al., "Electron-nuclear correlated multiphoton-route to Rydberg fragments of molecules," *Nat. Commun.* **10**(1), 757 (2019).
19. J. Ma et al., "Strong-field dissociative Rydberg excitation of oxygen molecules: electron-nuclear correlation," *Phys. Rev. A* **100**(6), 063413 (2019).
20. B.-B. Wang et al., "Coulomb potential recapture effect in above-barrier ionization in laser pulses," *Chin. Phys. Lett.* **23**(10), 2729–2732 (2006).
21. T. Nubbemeyer et al., "Strong-field tunneling without ionization," *Phys. Rev. Lett.* **101**(23), 233001 (2008).
22. T. Nubbemeyer, U. Eichmann, and W. Sandner, "Excited neutral atomic fragments in the strong-field dissociation of N_2 molecules," *J. Phys. B: At. Mol. Opt. Phys.* **42**(13), 134010 (2009).
23. J. McKenna et al., "Frustrated tunneling ionization during laser-induced D_2 fragmentation: detection of excited metastable D* atoms," *Phys. Rev. A* **84**(4), 043425 (2011).
24. J. McKenna et al., "Frustrated tunnelling ionization during strong field fragmentation of D_3^+," *New J. Phys.* **14**(10), 103029 (2012).
25. B. Ulrich et al., "Double-ionization mechanisms of the argon dimer in intense laser fields," *Phys. Rev. A* **82**(1), 013412 (2010).
26. B. Manschwetus et al., "Mechanisms underlying strong-field double ionization of argon dimers," *Phys. Rev. A* **82**(1), 013413 (2010).
27. J. Wu et al., "Multiple recapture of electrons in multiple ionization of the argon dimer by a strong laser field," *Phys. Rev. Lett.* **107**(4), 043003 (2011).
28. X. Xie et al., "Tunneling electron recaptured by an atomic ion or a molecular ion," *Phys. Rev. A* **88**(6), 065401 (2013).
29. S. Larimian et al., "Localizing high-lying Rydberg wave packets with two-color laser fields," *Phys. Rev. A* **96**(2), 021403 (2017).
30. W. Zhang et al., "Tracking the electron recapture in dissociative frustrated double ionization of D_2," *Phys. Rev. A* **98**(1), 013419 (2018).
31. S. Xu et al., "Observation of a transition in the dynamics of strong-field atomic excitation," *Phys. Rev. A* **102**(4), 043104 (2020).
32. H. Zimmermann et al., "Unified time and frequency picture of ultrafast atomic excitation in strong laser fields," *Phys. Rev. Lett.* **118**(1), 013003 (2017).
33. K. Lin et al., "Directional bond breaking by polarization-gated two-color ultrashort laser pulses," *J. Phys. B: At. Mol. Opt. Phys.* **49**(2), 025603 (2015).
34. C. A. Mancuso et al., "Controlling electron-ion rescattering in two-color circularly polarized femtosecond laser fields," *Phys. Rev. A* **93**(5), 053406 (2016).
35. J. L. Chaloupka and D. D. Hickstein, "Dynamics of strong-field double ionization in two-color counter-rotating fields," *Phys. Rev. Lett.* **116**(14), 143005 (2016).
36. C. A. Mancuso et al., "Controlling nonsequential double ionization in two-color circularly polarized femtosecond laser fields," *Phys. Rev. Lett.* **117**(13), 133201 (2016).
37. S. Eckart et al., "Nonsequential double ionization by counter-rotating circularly polarized two-color laser fields," *Phys. Rev. Lett.* **117**(13), 133202 (2016).
38. K. Lin et al., "Comparison study of strong-field ionization of molecules and atoms by bicircular two-color femtosecond laser pulses," *Phys. Rev. Lett.* **119**(20), 203202 (2017).
39. A. Fleischer et al., "Spin angular momentum and tunable polarization in high-harmonic generation," *Nat. Photonics* **8**(7), 543–549 (2014).
40. O. Kfir et al., "Generation of bright phase-matched circularly polarized extreme ultraviolet high harmonics," *Nat. Photonics* **9**(2), 99–105 (2015).
41. D. D. Hickstein et al., "Non-collinear generation of angularly isolated circularly polarized high harmonics," *Nat. Photonics* **9**(11), 743–750 (2015).
42. W. Zhang et al., "All-optical nanoscopic spatial control of molecular reaction yields on nanoparticles," *Optica* **9**(5), 551–560 (2022).
43. C. Cao et al., "Frustrated tunneling ionization in strong circularly polarized two-color laser fields," *J. Phys. B: At. Mol. Opt. Phys.* **54**(3), 035601 (2021).
44. G. P. Katsoulis, R. Sarkar, and A. Emmanouilidou, "Enhancing frustrated double ionization with no electronic correlation in triatomic molecules using counter-rotating two-color circular laser fields," *Phys. Rev. A* **101**(3), 033403 (2020).
45. R. Dörner et al., "Cold target recoil ion momentum spectroscopy: a 'momentum microscope' to view atomic collision dynamics," *Phys. Rep.* **330**(2–3), 95–192 (2000).
46. J. Ullrich et al., "Recoil-ion and electron momentum spectroscopy: reaction-microscopes," *Rep. Prog. Phys.* **66**(9), 1463–1545 (2003).
47. S. Alnaser et al., "Laser-peak-intensity calibration using recoil-ion momentum imaging," *Phys. Rev. A* **70**(2), 023413 (2004).
48. W. Zhang et al., "Photon-number-resolved asymmetric dissociative single ionization of H_2," *Phys. Rev. A* **96**(3), 033405 (2017).
49. S. Larimian et al., "Coincidence spectroscopy of high-lying Rydberg states produced in strong laser fields," *Phys. Rev. A* **94**(3), 033401 (2016).
50. H. Zimmermann et al., "Strong-field excitation of helium: bound state distribution and spin effects," *Phys. Rev. Lett.* **114**(12), 123003 (2016).
51. E. Diesen et al., "Dynamical characteristics of Rydberg electrons released by a weak electric field," *Phys. Rev. Lett.* **116**(14), 143006 (2016).
52. H. Lv et al., "Comparative study on atomic and molecular Rydberg-state excitation in strong infrared laser fields," *Phys. Rev. A* **93**(3), 033415 (2016).
53. W. Zhang et al., "Visualizing and steering dissociative frustrated double ionization of hydrogen molecules," *Phys. Rev. Lett.* **119**(25), 253202 (2017).

54. A. Azarm et al., “Neutral dissociation of hydrogen molecules in a strong laser field through superexcited states,” *J. Phys. B* **44**(8), 085601 (2011).
55. C. A. Mancuso et al., “Observation of ionization enhancement in two-color circularly polarized laser fields,” *Phys. Rev. A* **96**(2), 023402 (2017).
56. C. Guo et al., “Single and double ionization of diatomic molecules in strong laser fields,” *Phys. Rev. A* **58**(6), R4271–R4274 (1998).
57. B. Manschwetus et al., “Strong laser field fragmentation of H_2: Coulomb explosion without double ionization,” *Phys. Rev. Lett.* **102**(11), 113002 (2009).
58. A. Emmanouilidou et al., “Routes to formation of highly excited neutral atoms in the breakup of strongly driven H_2,” *Phys. Rev. A* **85**(1), 011402 (2012).
59. T. Zuo and A. D. Bandrauk, “Charge-resonance-enhanced ionization of diatomic molecular ions by intense lasers,” *Phys. Rev. A* **52**(4), R2511–R2514 (1995).
60. M. V. Ammosov, N. B. Delone, and V. P. Krainov, “Tunnel ionization of complex atoms and of atomic ions in an alternating electromagnetic field,” *Sov. Phys. JETP* **64**, 1191–1194 (1986).
61. N. Shvetsov-Shilovski et al., “Capture into Rydberg states and momentum distributions of ionized electrons,” *Laser Phys.* **19**(8), 1550–1558 (2009).
62. S. V. Popruzhenko, “Quantum theory of strong-field frustrated tunneling,” *J. Phys. B* **51**(1), 014002 (2018).
63. S. Hu et al., “Quantum dynamics of atomic Rydberg excitation in strong laser fields,” *Opt. Express* **27**(22), 31629–31643 (2019).
64. E. Olofsson, S. Carlström, and J. M. Dahlström, “Frustrated tunneling dynamics in ultrashort laser pulses,” *J. Phys. B* **54**(15), 154002 (2021).

Wenbin Zhang received his PhD in ultrafast optics, supervised by Prof. Jian Wu, from East China Normal University (ECNU) in 2020. Then, he worked at Ludwig-Maximilians-Universität, Munich and Max-Planck Institute of Quantum Optics, as a postdoctoral fellow supported by the Alexander von Humboldt Foundation and the Multiply fellowship program under the Marie Skłodowska-Curie Cofund Action. His research focuses on the laser-induced ultrafast physics of molecules and nanoparticles.

Yongzhe Ma received his bachelor's degree in physics from Yantai University. He is a PhD student, supervised by Dr. Hongcheng Ni, in Prof. Jian Wu's group, at East China Normal University. His main research interest is excitation and ionization of atoms and molecules in strong laser fields.

Chenxu Lu received his bachelor's degree in physics from Shanghai Normal University of China. He is a PhD student, supervised by Professor Jian Wu, at East China Normal University. His main research interest is laser-induced ultrafast dynamics.

Fei Chen is a PhD candidate at State Key Laboratory of Precision Spectroscopy, East China Normal University, supervised by Prof. Jian Wu. His research focuses on the ultrafast dynamics of room temperature microcavity exciton-polariton.

Shengzhe Pan is a PhD student, supervised by Prof. Jian Wu, at East China Normal University, where he received his bachelor's degree in physics. His main research interest is ultrafast molecular dynamics in strong laser fields.

Peifen Lu: Biography is not available.

Hongcheng Ni is a research professor leading a theoretical division within the group of Prof. Jian Wu. He received his PhD from University of Colorado, and subsequently did his postdoctoral research at the Max Planck Institute for the Physics of Complex Systems as a Humboldt fellow and at the Vienna University of Technology as a Meitner fellow. His primary research interest is ultrafast and strong-field physics.

Jian Wu is a professor at the State Key Laboratory of Precision Spectroscopy, East China Normal University (ECNU), Shanghai, China. He received his PhD from ECNU, and did his postdoc as an Alexander von Humboldt research fellow at Goethe University Frankfurt. His research focuses on the measurement and control of the ultrafast dynamics of molecules in strong laser fields.